



1 **Carbon reduction requires attention to the contribution of natural gas use: Combustion and**  
2 **leakage**

3 Haoyuan Chen<sup>1,5</sup>, Tao Song<sup>1,5\*</sup>, Xiaodong Chen<sup>2</sup>, Yinghong Wang<sup>1</sup>, Mengtian Cheng<sup>1</sup>, Kai Wang<sup>1</sup>,  
4 Fuxin Liu<sup>4</sup>, Baoxian Liu<sup>3</sup>, Guiqian Tang<sup>1,5\*</sup>, Yuesi Wang<sup>1,5</sup>

5 Correspondence to Guiqian Tang (tgq@dq.cern.ac.cn) Tao Song (st@dq.cern.ac.cn)

6 1. Key Laboratory of Atmospheric Environment and Extreme Meteorology, Institute of  
7 Atmospheric Physics, Chinese Academy of Sciences, Beijing, 100029, China

8 2. Beijing Aozuo Ecological Instrument Co., Ltd., Beijing 100080, China

9 3. Beijing Key Laboratory of Airborne Particulate Matter Monitoring Technology, Beijing  
10 Municipal Environmental Monitoring Center, Beijing, 100048, China

11 4. Anhui University of Science and Technology, Anhui 232001, China

12 5. University of Chinese Academy of Sciences, Beijing 100049, China  
13

14 Abstract: Natural gas will continue to replace coal in the process of global energy structure reform,  
15 but its leakage potential can delay the realization of global carbon neutrality. To quantify its  
16 impact, we established a carbon dioxide (CO<sub>2</sub>) and methane (CH<sub>4</sub>) emission flux detection  
17 platform on the 220-m platform of the Institute of Atmospheric Physics, Chinese Academy of  
18 Sciences, located in northwestern Beijing. The observation results indicated that the daily mean  
19 CO<sub>2</sub> and CH<sub>4</sub> fluxes were  $12.21 \pm 1.75 \mu\text{mol}\cdot\text{m}^{-2}\cdot\text{s}^{-1}$  and  $95.54 \pm 18.92 \text{ nmol}\cdot\text{m}^{-2}\cdot\text{s}^{-1}$ , respectively.  
20 The daily variations in the emissions of these two gases were highly consistent, and their fluxes  
21 were significantly correlated with natural gas consumption, indicating that natural gas has become  
22 a common source of CH<sub>4</sub> and CO<sub>2</sub>. Vehicle-based identification demonstrated that methane can  
23 escape at the storage and use stages of natural gas. Based on natural gas consumption data, the  
24 upper limit of the calculated natural gas leakage rate in Beijing reached  $1.12 \pm 0.22\%$ , indicating  
25 that the contribution of CH<sub>4</sub> to climate change could reach 23% of that of CO<sub>2</sub> on a 20-year scale.  
26 Natural gas leakage was estimated to delay the time for China to achieve carbon neutrality by  
27 almost three years.

28 **KEY WORDS:**

29 CO<sub>2</sub> flux, CH<sub>4</sub> flux, Eddy covariance, Natural gas leakage, Climate forcing, Carbon neutrality



30 **1. INTRODUCTION**

31 In 2015, the 1.5°C temperature control target was proposed in the Paris Agreement to reduce  
32 the occurrence of extreme weather events. To achieve this goal, it is necessary to actively promote  
33 the low-carbon development transformation of the economic system, especially energy  
34 transformation. In this process, natural gas plays an important role, and typical countries have  
35 indicated a trend of coal reduction and gas increase during energy structure adjustment over the  
36 past century. It is expected that global natural gas consumption will continue to increase by 2035.

37 Natural gas is commonly referred to as a clean alternative to coal, but its main component is  
38 methane, with a global warming potential (GWP) that is 29.8 times greater than that of carbon  
39 dioxide at the hundred-year scale.<sup>1</sup> If 3.4% of methane leaks into the atmosphere before natural  
40 gas combustion, the advantages of natural gas over coal will become negligible.<sup>2</sup> Recent studies  
41 have suggested that the average loss rate of natural gas in cities worldwide ranges from 3.3% to  
42 4.7%.<sup>3</sup> According to statistics from the International Energy Agency ([www.iea.org](http://www.iea.org)) in 2020,  
43 methane leakage in the global oil and gas industry reached 72 million tons and amounted to 6  
44 billion tons of carbon dioxide equivalent (CO<sub>2</sub>e) within 20 years. Therefore, it is unclear whether  
45 natural gas can become a bridging material for energy transformation.

46 One important prerequisite is to determine the contribution of natural gas leakage during  
47 coal-to-gas conversion to urban methane emissions and its climate effects. At present,  
48 conventional methane monitoring methods include ground, aviation, and satellite monitoring  
49 methods. Ground monitoring aims to detect the atmospheric methane concentration through the  
50 installation of sensors and monitoring stations at fixed locations or on vehicles.<sup>4</sup> Notably,  
51 monitoring equipment is often installed near potential emission sources, with high detection  
52 accuracy but generally a limited spatial range. The aviation monitoring method can be employed  
53 to identify large-scale methane emissions through measurement techniques such as drones or  
54 aircraft but cannot be used to achieve long-term monitoring.<sup>5-7</sup> Satellite methods can compensate  
55 for the shortcomings of the former two methods,<sup>8-10</sup> which exhibit interference from clouds and  
56 require significant labor and financial investments.

57 The eddy covariance method, which is based on tall towers, enables long-term monitoring of  
58 methane emissions, thus facilitating the identification of methane sources in specific areas.  
59 However, it should be noted that this method has certain limitations during urban flux



60 measurements at higher altitudes, as larger air volumes in the measurement system may lead to a  
61 significant imbalance between the observed vertical turbulence exchange and surface net flux  
62 compared with those at typical measurement heights. However, this deficiency should be  
63 considered in conjunction with the advantages of urban tower measurements because cities  
64 typically correspond to deeper rough sublayers that can extend to 2–5 times the average building  
65 height.<sup>11</sup> Therefore, increasing the measurement altitude can help characterize the turbulent  
66 exchange between this layer and the inertial sublayer.

67 Developing countries are the main driving force behind the continuous growth in global  
68 energy demand. As Beijing is the capital of the world's largest developing country and the first  
69 city within China to complete the coal-to-gas conversion process, clarifying the natural gas  
70 leakage process in Beijing can provide guidance for energy transformation in developing countries  
71 regionally and even globally. In this study, three aspects related to natural gas were investigated as  
72 follows. First, the fluxes of methane and carbon dioxide were observed simultaneously via the  
73 eddy covariance method, which was used to investigate the impact of the coal-to-gas policy on  
74 carbon dioxide and methane in Beijing, including the magnitude of carbon dioxide emission and  
75 the common effects on the sources of both. Second, with navigation experiments, the natural gas  
76 leakage process in Beijing has been confirmed, and the emission levels of natural gas at different  
77 stages have been further roughly estimated, which provides certain effective insights for the  
78 control of natural gas leakage in Beijing. Third, we discuss climate forcing caused by natural gas  
79 leakage while considering the carbon dioxide flux as a basis, calculate the natural gas leakage rate  
80 with statistical data, and estimate the impact of natural gas leakage on China's carbon peak and  
81 carbon neutrality in conjunction with existing reports.

82

## 83 **2. METHODS**

### 84 **2.1 Instrument setup for eddy covariance measurement**

85 The measurements were conducted at a 325-m high meteorological tower in northwestern  
86 Beijing, with a closed-path observation system installed on a platform at a height of 220 m, which  
87 included a dual laser gas analyzer (QC-TILDAS-DUAL, Aerodyne Research Inc., USA),



88 three-dimensional ultrasonic anemometer (Gill Instruments, Ltd., Lymington, Hampshire, UK),  
89 vacuum pump (XDS35i, BOC Edwards, UK), data collector (CR6, Campbell Scientific Inc., USA),  
90 and other accessories. In the dual laser gas analyzer, tunable infrared laser direct absorption  
91 spectroscopy (TILDAS) technology is used to detect the most significant fingerprint transition  
92 frequencies of molecules within the mid-infrared wavelength range. The analyzer has an optical  
93 path of up to 76 m and can measure H<sub>2</sub>O, CO<sub>2</sub> and CH<sub>4</sub> simultaneously. Similar instruments have  
94 been applied to observe outdoor ecosystems.<sup>12</sup> Under the action of a vacuum pump, the air sample  
95 enters the instrument room at a flow rate of 2 lpm through a polytetrafluoroethylene (PTFE)  
96 sampling tube with a length of 3 m and an inner diameter of 3 mm (Figure S1). Instrument  
97 calibration includes zero-point and range calibration processes. High-purity nitrogen gas  
98 (>99.999%) was used for zero-point calibration at 1-hour intervals. In this process, the  
99 corresponding solenoid valve was opened, which was automatically controlled by TDLWintel  
100 software, and range calibration was performed at the factory. In addition, before the experiment,  
101 we calibrated the gas analyzer using CO<sub>2</sub> (401 ppm) and CH<sub>4</sub> (219 ppb) standard gases. We found  
102 that the measured and standard gas concentrations differed by less than 1%, indicating satisfactory  
103 instrument performance. Therefore, we did not perform range calibration later. The instrument was  
104 placed in an insulated box equipped with air conditioning to ensure normal operation of the laser.  
105 Both instruments were operated at a sampling frequency of 10 Hz. The data collector and  
106 high-frequency instrument were timed according to the network and global positioning system  
107 (GPS), respectively, to maintain synchronization. To minimize the twisting effect of the flux tower  
108 on the incoming air, a three-dimensional ultrasonic anemometer was installed at the end of a 1.5-m  
109 long support arm facing southeast China in summer. This measurement lasted from June 11 to  
110 September 7, 2022, during which the nitrogen cylinder was replaced, and the instrument was  
111 debugged on June 18 and 19. From July 12 to 26, the experiment was stopped due to failure of the  
112 tower power supply.

## 113 **2.2 Flux data processing**

114 The flux data processing operation in this study is based on the eddy covariance technique  
115 via EddyPro software (version 6.2.1, Li COR, Inc.; Lincoln, Nebraska, USA). An average flux



116 calculation period of 30 minutes was selected.<sup>13</sup> Before calculating half-hourly fluxes, spike  
117 detection and data rejection algorithms were applied using dynamic mean and standard deviation  
118 values within a series of moving windows, as described by Vickers and Mahrt.<sup>14</sup> The double  
119 rotation method proposed by Kaimal and Finnigan<sup>15</sup> was employed for tilt correction. The delay  
120 time caused by the spatial separation of gas analyzers and three-dimensional ultrasonic  
121 anemometers (as well as the injection pipeline of closed-path systems) was corrected via the  
122 maximum covariance method.<sup>16</sup> Webb, Pearman, and Leuning (WPL) correction was not applied  
123 here<sup>17</sup> because the instrument room was in a constant temperature and pressure state that  
124 converted the real-time concentration into a dry volume mixing ratio, and the longer pipeline of  
125 the closed-path system avoided the influence of temperature fluctuations. The limitations of eddy  
126 covariance systems can lead to frequency loss in flux observations. Factors such as a limited  
127 average period and linear detrending can cause low-frequency loss, whereas instrument separation,  
128 path averaging, insufficient high-frequency responses, and pipeline attenuation can cause  
129 high-frequency loss. The method proposed by Moncrieff et al<sup>18</sup> was employed for frequency  
130 response correction. After the above correction of the flux data, in this paper, the 0-1-2 quality  
131 labeling scheme proposed by Mauder and Foken<sup>19</sup> was adopted for data quality control purposes.  
132 Notably, a value of 0 represents data with the best quality, a value of 1 represents data with good  
133 quality, and a value of 2 represents data with poor quality. In this study, flux data marked as 2  
134 were excluded from the subsequent analysis. In addition, the flux source area was evaluated via  
135 the method of Kljun et al. (Text. S1),<sup>20</sup> and the flux source area covers most of the urban area of  
136 Beijing and reflects the average emission characteristics at the regional scale.

### 137 **2.3 Spectral analysis**

138 High-frequency signal loss can occur in closed-path systems. To determine the response  
139 capability of the closed-path system to high-frequency turbulence signals, we analyzed the  
140 observed gas exchange signals through the turbulence power spectrum. The selected time ranges  
141 from 12:00 to 16:00 every day during the observation period, with a total of 8 and a half hours of  
142 data. The data were integrated and averaged, and the data curve was then compared with the ideal  
143 slope in the inertia subarea (Figure S2).  $\text{Co}(wT)$  followed the theoretical  $f_n^{-4/3}$  (where  $f_n$  denotes the



144 normalized frequency) in the inertial subregion. In contrast, the slopes of  $\text{Co}(w\text{CO}_2)$  and  $\text{Co}(w\text{CH}_4)$   
145 were slightly greater than  $-4/3$ , indicating that there was high-frequency loss in the flux  
146 observations of the closed-loop system.<sup>21</sup> Through high-frequency correction, the calculation  
147 results indicated that the  $\text{CO}_2$  and  $\text{CH}_4$  fluxes were 7.73% and 6.85% greater, respectively, than  
148 those before correction.

149

150

#### 151 **2.4 Mobile $\text{CH}_4$ and $\text{CO}_2$ observations**

152 Vehicle-based experiments were conducted in the urban area of Beijing in the winter of 2023  
153 and the summer of 2024, and the specific deployment of the mobile observation station is shown  
154 in Figure S1. Notably, the car was equipped with a  $\text{CO}_2/\text{CH}_4$  spectrometer (Los Gatos Research,  
155 Inc., USA), a laptop for data viewing, and a mobile power supply (Figure S3). Zero-point  
156 calibration of the instrument was performed once pure nitrogen was used before the mobile  
157 experiment began. Standard gases of methane and carbon dioxide were introduced to calibrate the  
158 instrument simultaneously, and we found that the concentration of the instrument matched well  
159 with the standard gas. Since we focused more on the enhancement in concentration rather than  
160 itself, we did not calibrate it again afterward. The sampling port was located approximately 20 cm  
161 from the roof, and ambient air was collected through a PTFE tube with a length of 2 m and an  
162 inner diameter of 3 mm. Before the particulate matter entered the instrument, it was removed  
163 using a filter head. The IMET sounding instrument (International Met Systems, USA) is installed  
164 on the roof, with a sampling frequency that is consistent with that of the other instruments, i.e., 1 s,  
165 real-time concentration information of different latitudes and longitudes is obtained at a resolution  
166 of seconds through the corresponding time between the GPS and the instrument; for example, if  
167 the GPS sampling time delay is 3 s, the latitude and longitude coordinates are reassigned to the  
168  $\text{CH}_4$  reading observed three seconds prior. Our observation sites include petrochemical plants  
169 located in southwestern Beijing, natural gas storage tanks and landfills in the northeastern part,  
170 and power plants with the highest natural gas usage in the southeastern part.

171



172

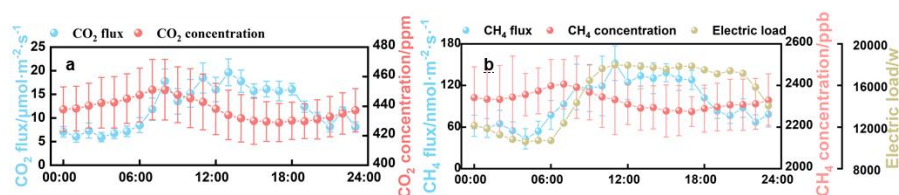
### 173 3. RESULTS

#### 174 3.1 Diurnal variation in the flux

175 A positive or negative flux reflects the vertical exchange direction of trace gases in the urban  
176 canopy, which is positive upward and negative downward. (The uncertainty analysis is described  
177 in the Text. S2 and Figure S4, respectively) Overall, both CO<sub>2</sub> and CH<sub>4</sub> fluxes are positive on a  
178 daily scale, indicating that cities are the source of both gases. The mean diurnal CO<sub>2</sub> flux is 12.21  
179  $\pm 1.75 \mu\text{mol}\cdot\text{m}^{-2}\cdot\text{s}^{-1}$  (ranging from 6.05 to 19.66  $\mu\text{mol}\cdot\text{m}^{-2}\cdot\text{s}^{-1}$  (Figure 1a), which is generally  
180 lower than that at 200 m in summer from 2013 to 2016 (mean 14.45  $\mu\text{mol}\cdot\text{m}^{-2}\cdot\text{s}^{-1}$ , ranging  
181 between 5 and 30  $\mu\text{mol}\cdot\text{m}^{-2}\cdot\text{s}^{-1}$ )<sup>22</sup>, and at 140 m in summer from 2006 to 2009 (mean 16.19  $\pm 4.12$   
182  $\mu\text{mol}\cdot\text{m}^{-2}\cdot\text{s}^{-1}$ , ranging from 8 to 20  $\mu\text{mol}\cdot\text{m}^{-2}\cdot\text{s}^{-1}$ )<sup>23</sup>, a smaller deviation suggests that carbon  
183 dioxide may be dominated by a more stable source than before. We also obtained observation  
184 results at 140 m in summer from 2009–2017.<sup>24</sup> The flux in 2022 significantly decreased compared  
185 with previous levels (Figure S5), which reflects the transformation of Beijing's energy structure.  
186 The coal-to-gas policy implemented by Beijing these years led to a gradual decrease in the  
187 proportion of coal in primary energy consumption, with a steady increase in the proportion of  
188 natural gas in total consumption (Figure S6), the use of natural gas results in much less coal  
189 carbon dioxide than coal, generating the same amount of heat; moreover, Beijing has increased the  
190 amount of electricity flow from other provinces in recent years (Figure S6), which has further  
191 driven a decrease in the annual average concentration of PM<sub>2.5</sub>, which is expected to decrease to  
192 30  $\mu\text{g}\cdot\text{m}^{-3}$  by 2022. In fact, previous studies have reported a high correlation between PM<sub>2.5</sub> and  
193 CO<sub>2</sub> fluxes. For example, Donato et al<sup>25</sup>. found that the seasonal and daily variations in the  
194 particle number flux in southern Italian suburbs are largely determined by both transportation  
195 activities and household heating. Liu et al<sup>24</sup> confirmed that the CO<sub>2</sub> flux can explain 64% of the  
196 interannual variation in the PM<sub>2.5</sub> concentration by fitting the correlation between the annual  
197 average PM<sub>2.5</sub> and CO<sub>2</sub> fluxes in Beijing from 2009 to 2017. Therefore, controlling CO<sub>2</sub> emissions  
198 can also greatly control the concentration level of PM<sub>2.5</sub>, thus achieving the dual effects of  
199 mitigating climate change and improving air quality. In terms of its diurnal variation, it did not



200 follow a typical bimodal pattern but rather remained high after reaching the first peak at 8:00, with  
 201 a lower level at night, reflecting high anthropogenic carbon emissions during the day, such as  
 202 those resulting from transportation and energy generation activities. The diurnal pattern of the CH<sub>4</sub>  
 203 flux was similar to the observation results of Giolo et al<sup>26</sup> and Helfer et al<sup>27</sup> (Figure 1b), reflecting  
 204 an increase in emissions during the day. The CH<sub>4</sub> flux rapidly increased from approximately 5:00  
 205 and reached a peak of 152.15 nmol·m<sup>-2</sup>·s<sup>-1</sup> at approximately 12:00. Notably, after 17:00, it begins  
 206 to decrease. Assuming that the average methane flux at midnight (00:00 to 06:00) can be  
 207 employed as the baseline for nighttime emissions, which accounts for 58% of the daily average  
 208 flux, the methane flux did demonstrate a pronounced diurnal pattern, indicating a significant daily  
 209 variation in the background source in the source area.



210  
 211 Figure 1 Daily variations in the CO<sub>2</sub> and CH<sub>4</sub> concentrations, fluxes, and electricity loads

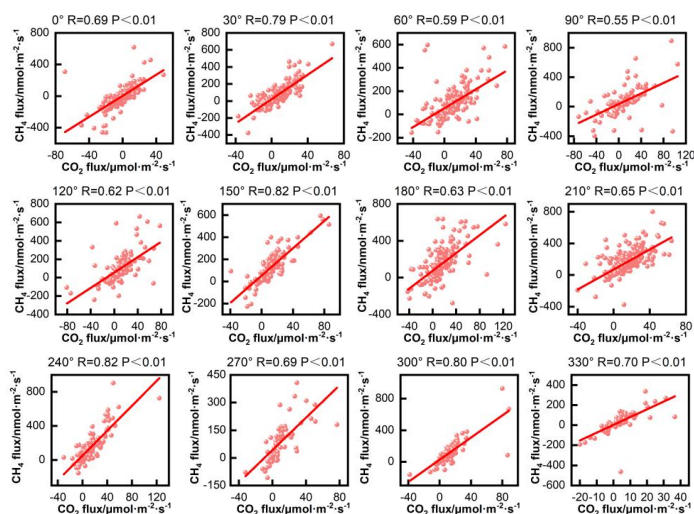
### 212 3.2 Homology between CO<sub>2</sub> and CH<sub>4</sub>

213 The CO<sub>2</sub> fluxes exhibited similar diurnal patterns to the CH<sub>4</sub> fluxes, with the midnight mean  
 214 accounting for 54% of the daily mean, which suggests that the fluxes may be driven by the same  
 215 emission source. From the perspective of correlation statistics, the CO<sub>2</sub> and CH<sub>4</sub> fluxes showed a  
 216 significant correlation along all directions (Figure 2), with correlation coefficients greater than that  
 217 at the center of Loz, Poland (0.50),<sup>28</sup> but the low correlation between the CO<sub>2</sub> and CH<sub>4</sub> fluxes and  
 218 the temperature excludes the conclusion that biological sources dominate their emissions.  
 219 Therefore, CO<sub>2</sub> and CH<sub>4</sub> share the same anthropogenic sources within the source area. This  
 220 homology is also reflected in their spatial distributions, with high fluxes mainly distributed south  
 221 of the tower, which is more densely populated and encompasses complex industrial structures, and  
 222 much lower fluxes in the northern forest and park areas (Figure 3a, b). The correlation between the  
 223 spatial distributions of the CO<sub>2</sub> and CH<sub>4</sub> fluxes reached 0.98, demonstrating the common impact of  
 224 similar anthropogenic sources on their emissions. The linear fitting results at 150° and 240°





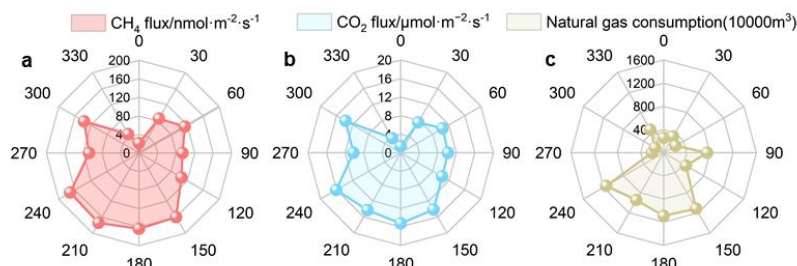
225 indicated the highest correlation coefficient (0.82) along all directions (Figure 2), further  
226 supporting this viewpoint.  
227



228

229

Figure 2 Linear fitting results for the CH<sub>4</sub> and CO<sub>2</sub> fluxes in the 12 directions



230

231

232

233

Figure 3 Mean CH<sub>4</sub> and CO<sub>2</sub> concentrations, fluxes and natural gas consumption in the 12 directions

## 234 DISCUSSION

### 235 3.3 Driver of the homology between CO<sub>2</sub> and CH<sub>4</sub>

236 After the introduction of natural gas in 1985, the proportion of natural gas in the fossil fuel  
237 industry of Beijing increased annually, especially when coal was replaced with natural gas and  
238 electricity in 2014 and 2018, respectively, and natural gas became the most consumed fossil fuel



239 (Figure 4a). According to the 2022 Beijing Statistical Yearbook  
240 (<https://nj.tjj.beijing.gov.cn/nj/main/2023-tjnj/zk/e/indexch.htm>), natural gas is used mainly for  
241 thermal power generation and heating (accounting for 69%). Owing to the low proportion of  
242 heating in summer, natural gas in Beijing is mostly used for thermal power generation in summer.  
243 Owing to the difficulty in obtaining hourly electricity generation data, we obtained a daily  
244 variation curve of the electricity load in Beijing based on the statistical data (power plants usually  
245 calculate the required electricity generation based on the electricity load)  
246 ([https://www.gov.cn/zhengce/zhengceku/2020/12/03/5566580/files/eaaa93782e514543861bdcd43](https://www.gov.cn/zhengce/zhengceku/2020/12/03/5566580/files/eaaa93782e514543861bdcd434e86666.pdf)  
247 [4e86666.pdf](https://www.gov.cn/zhengce/zhengceku/2020/12/03/5566580/files/eaaa93782e514543861bdcd434e86666.pdf)) (Figure 1b). The daily variation in the electricity load is highly consistent with that  
248 in the CH<sub>4</sub> flux, with the maximum CH<sub>4</sub> flux occurring at 11:00 pm during the peak electricity  
249 consumption period. After 16:00 pm, the electricity load and CH<sub>4</sub> flux decrease synchronously.  
250 Thus, the daily variation in the CH<sub>4</sub> flux is driven by natural gas consumption. We gridded the  
251 natural gas consumption data (Figure S8) and calculated the mean natural gas consumption along  
252 all directions within the flux source area (Figure 3c). Notably, a high consistency between the  
253 spatial distributions of the CO<sub>2</sub> and CH<sub>4</sub> fluxes and natural gas consumption was found, which  
254 reflects that after the adjustment of the energy structure in Beijing, natural gas became the main  
255 source of CO<sub>2</sub> and CH<sub>4</sub>. Considering the high photosynthetic absorption of CO<sub>2</sub> by plants in  
256 summer, this conclusion also applies to the other seasons, which supports the hypothesis that  
257 natural gas is the main source of winter CO<sub>2</sub> emissions in Beijing, as determined based on the  
258 isotope tracing method.<sup>29,30</sup>

259 To confirm this conclusion and explain the main processes of natural gas leakage,  
260 vehicle-based observations were obtained near large petrochemical plants, gas storage tanks, and  
261 power plants in Beijing in both winter and summer. Owing to the influence of weather conditions  
262 and pollution transport, the concentration of gases can change at any time. To remove these effects,  
263 a certain method is needed to determine the background value at each moment. Following the  
264 approach of Pu et al.,<sup>31</sup> we divided the time series into discrete 5-minute windows and located the  
265 5th percentile concentration in each window as the background value. The enhancement  
266 concentration can be defined as the difference between the observed value and the background  
267 value at the corresponding time. There was significant methane leakage around the gas storage  
268 tanks and power plants in both winter and summer. Notably, the observed methane hotspots were



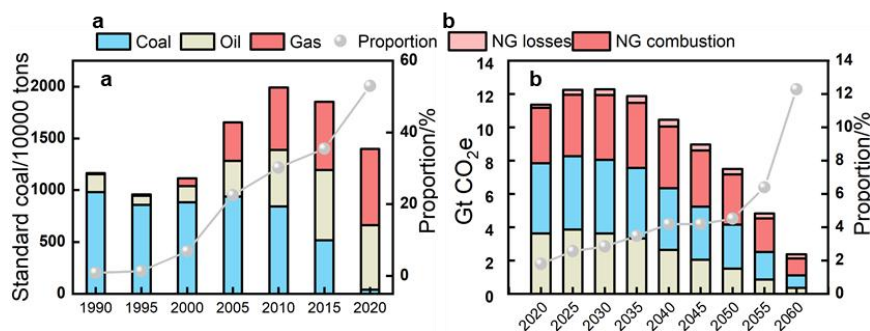
269 located in the downzone of potential leakage sources; therefore, we attribute the high methane  
270 concentration to the emissions of these potential natural gas leakage sources. In winter, hotspots  
271 with concentrations higher than the background value of 1763 ppb appeared around the gas  
272 storage tank (Figure 5a), corresponding to an E-CH<sub>4</sub> and E-CO<sub>2</sub> fingerprint line with a slope of  
273 0.14 (Figure 6a). In addition, the enhancement concentration fingerprint slopes of the other  
274 hotspot zones were 0.25 and 0.05, respectively, indicating varying degrees of leakage around the  
275 gas storage tank.<sup>32</sup> The enhancement concentration fingerprint in summer also revealed leakage  
276 related to gas storage equipment (Figure 5b), with a slope of 0.03, similar to that of 0.05 in winter.  
277 Similar to gas storage tanks (Figure 6b), natural gas leakage hotspots have been observed in  
278 various equipment in power plants. For example, fingerprints with a slope of 0.025 in winter and  
279 summer reflected leakage related to gas storage facilities in power plants,<sup>33</sup> whereas fingerprints  
280 with a slope of 0.006 in summer reflected leakage related to combustion facilities (Figure 6d).<sup>34</sup>  
281 However, the observation results near the petrochemical plant seemed different from those above  
282 because the dispersion of E-CO<sub>2</sub> and E-CH<sub>4</sub> was very concentrated, making it difficult to  
283 discriminate obvious fingerprint profiles (Figure 6e). Combined with Chen et al.'s investigation  
284 into natural gas sources in China,<sup>8</sup> methane leakage from the production end is thought to be  
285 relatively small compared with that of other processes. As important sources of methane, landfills  
286 have received widespread attention, so we also conducted mobile observations near a large landfill  
287 outside the Fifth Ring Road in Beijing, which was a hotspot exhibiting a level exceeding the  
288 minimum concentration of 1385 ppb (Figure 5f). The concentration fingerprints were relatively  
289 disordered and significantly differed from those of methane emissions dominated by natural gas  
290 (Figure 6f), indicating that waste disposal processes are relatively complex and cannot be ignored  
291 in cities.<sup>35</sup>

292       Converting observed concentration increments into emission rates is a simple means of  
293 quantifying natural gas leakage, which is subject to atmospheric conditions and potential leak  
294 source locations. Well et al.<sup>36,37</sup> developed a model based on the relationship between the  
295 enhancement concentration and emission rate. The specific formula is shown in Text S5. The  
296 model assumes that CH<sub>4</sub> enhancement is the best predictor of the leakage emission rate and that a  
297 greater leakage emission rate corresponds to greater CH<sub>4</sub> enhancement. The method sets a  
298 minimum threshold for the observed methane concentration, which is 110% of the background



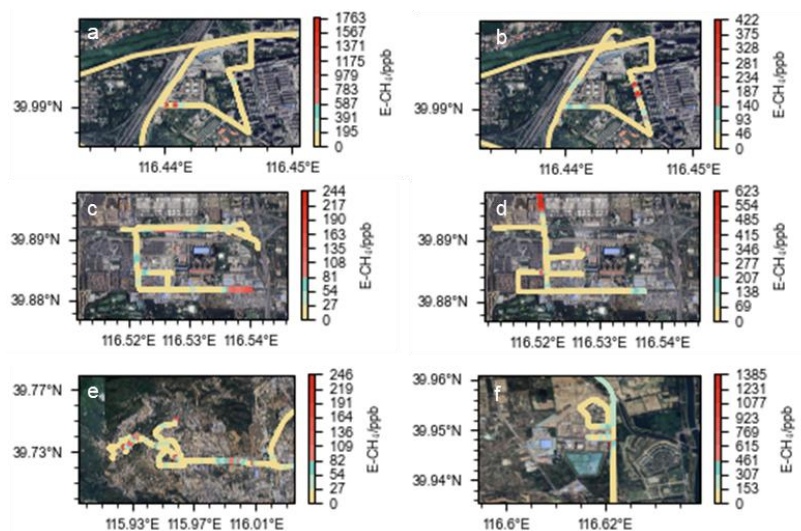
299 value, to filter out concentration changes caused by measurement. Moreover, when multiple  
 300 detections are conducted for the same leakage source, it is necessary to average the methane  
 301 enhancement values and then substitute them into the above formula. We estimated the natural gas  
 302 leakage emission rates from different leakage sources with this method. The type of concentration  
 303 fingerprint can help define the types of leakage sources. The methane leakage rates from gas  
 304 storage tanks and power plants during winter observation were calculated as 1.02–4.10 g/min and  
 305 0.41–0.57 g/min, respectively, and 0.98 g/min and 0.52–1.45 g/min, respectively, during summer,  
 306 which are lower than the results of Ars et al. on the leakage rates of Toronto's natural gas  
 307 distribution network (3.52–10.56 g/min),<sup>38</sup> but they noted that Well's method underestimated the  
 308 leakage rates because they ignored smaller concentration enhancements. A significant uncertainty  
 309 in this method lies in the distance between the leakage point and the vehicle; unfortunately,  
 310 determining the distance between the two points in practical operation is difficult, which may  
 311 confound the estimation of methane leakage. Therefore, sufficient mobile experiments should be  
 312 conducted in subsequent work to accurately calculate natural gas leakage in Beijing.

313



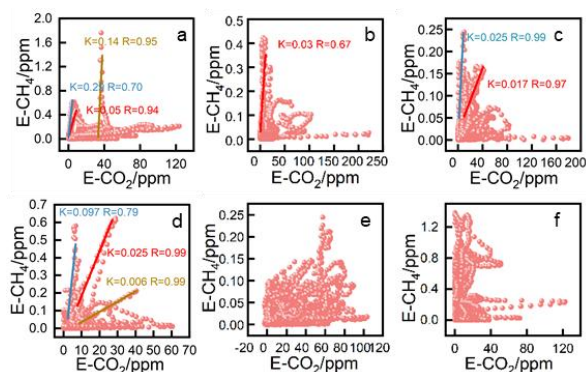
314  
 315 Figure 4 Terminal consumption of coal, oil, and natural gas and their proportions from 1990 to  
 316 2020(a) Since diesel-powered trucks are allowed only at night on the Fifth Ring Road and  
 317 kerosene, which is used mainly in aviation and is not included in the flux source area, oil mainly  
 318 comprises gasoline in this case), CO<sub>2</sub> equivalent from coal, oil and natural gas (losses and  
 319 combustion) in the future scenario (estimated by China Energy Outlook 2060 released by  
 320 SINOPEC in 2021), and CO<sub>2</sub> equivalent of natural gas leakage as a proportion of natural gas (NG)  
 321 combustion emissions(b)

322



323

324 Figure 5 Methane enhancement concentration vehicle-based results (a, c show storage tanks and  
 325 thermal power plants in winter; b, d show storage tanks and thermal power plants in summer; e  
 326 shows petrochemical plants; and f shows waste disposal stations)(all maps were extracted from  
 327 © Google earth: <https://earth.google.com/>)



328

329 Figure 6 Fitting of the CO<sub>2</sub> and CH<sub>4</sub> concentration enhancement values (a, c show the fitting  
 330 results for the gas storage tanks and power plants in winter; b, d show the fitting results for the gas  
 331 storage tanks and power plants in summer; e shows the petrochemical plants; and f shows the  
 332 waste disposal stations. Different fitting lines represent various leakage sources.)

### 333 3.4 Climatic effects of natural gas (NG) losses and their impact on carbon neutrality

334 Based on the natural gas consumption and flux data for the flux source area, the estimated  
 335 upper limit of the methane leakage rate in Beijing reached  $1.12 \pm 0.22\%$  (Text. S3), the lower limit  
 336 of natural gas leakage in Beijing is estimated to be 0.82%, considering the emissions from



337 biogenic sources (Text. S4), which is lower than the value of 2.07% calculated based on the  
338 purchase and sales statistics and the statistical mean value of 1.1–1.65% reported by the American  
339 Petroleum Institute (<https://www.api.org/>), we assume that the leakage rate does not have  
340 significant seasonal variability because of the positive correlation between methane flux and  
341 natural gas consumption. The natural gas leakage rate in Beijing is relatively low, as noted in  
342 existing reports. Nevertheless, the contributions of CH<sub>4</sub> to climate warming are 8.37% and 23.17%  
343 of those of CO<sub>2</sub> at the 100- and 20-year scales, respectively, according to the determined CO<sub>2</sub> and  
344 CH<sub>4</sub> fluxes and the GWP of methane. With the arrival of the winter heating season, climate forcing  
345 will further increase on a yearly scale. Assuming that the natural gas consumption amount in  
346 Beijing during the heating season is 5 times greater than that during the other seasons (according  
347 to Beijing Gas in 2019), that oil consumption does not significantly fluctuate throughout the year  
348 and that both the CO<sub>2</sub> and CH<sub>4</sub> fluxes are positively correlated with fossil fuel consumption and  
349 natural gas leakage, the climate forcing effect of natural gas leakage in 2022 is 11.47% on a  
350 100-year scale and can reach as high as 31.56% on a 20-year scale. However, when the same  
351 amount of heat is generated, the use of natural gas can yield CO<sub>2</sub> emission reductions of 50%  
352 relative to coal and of only approximately 30% relative to oil. Therefore, the reduction in  
353 greenhouse gas emissions resulting from natural gas combustion compared with that resulting  
354 from the combustion of other fossil fuels may be offset by the climate forcing effect of methane  
355 leakage in the short term, thus making it difficult for natural gas to become a transitional energy  
356 source for energy transition.

357 Numerous institutions have used carbon emission models to estimate carbon dioxide  
358 emissions in China under the scenarios of peaking carbon emissions by 2030 and achieving carbon  
359 neutrality by 2060. We used the results of the Global Climate Governance Strategy and China's  
360 Carbon Neutrality Path Outlook,<sup>39</sup> which indicate that carbon dioxide emissions in China under the  
361 carbon neutrality scenario reach approximately 2.1 Gt. Considering that carbon neutrality refers to  
362 the offsetting of greenhouse gas emissions and absorption, it is necessary to consider the leakage  
363 effect of natural gas. We calculated methane leakage in the corresponding year based on the  
364 natural gas consumption level under the future scenario of the China Energy Outlook 2060  
365 (SINOPEC 2021)<sup>40</sup> and the upper leakage rate obtained in this study and converted the value into  
366 carbon dioxide equivalents (CO<sub>2</sub>e) according to the GWP on a 20-year scale (Figure 4b). After



367 accounting for the natural gas leakage process, CO<sub>2e</sub> in China will still peak by 2030, but CO<sub>2e</sub>  
368 due to natural gas leakage will reach 0.26 Gt in 2060, accounting for 12% of the total CO<sub>2</sub>  
369 emissions (ignoring natural gas leakage) and 26% of the total CO<sub>2</sub> emissions resulting from  
370 natural gas combustion, which is comparable to the CO<sub>2</sub> emissions resulting from coal combustion  
371 (0.35 Gt). As natural carbon sinks do not notably fluctuate in the short term, the increase in carbon  
372 sinks in the future will depend mainly on carbon capture and storage (CCS) technology. It can be  
373 expected that at the current estimated CO<sub>2</sub> capture rate (0.1 Gt/year) (estimated by the China  
374 Energy Outlook 2060) (SINOPEC 2021) of CCS technology, the realization of carbon neutrality in  
375 China will be delayed by almost three years, so the leakage effect of natural gas must be  
376 considered along with the use of carbon modeling to determine future natural gas consumption  
377 levels.

378 Notably, the Beijing–Tianjin–Hebei region has experienced the most severe air pollution in  
379 China. To ensure people's health, Beijing's coal-to-gas policy has been implemented most  
380 thoroughly with a well-established layout and control measures for natural gas leakage across  
381 China, so it is reasonable to apply the leakage rate from Beijing to all of China and attempt to  
382 estimate the impact of natural gas leakage on China's carbon peak and carbon neutrality. Even  
383 though the natural gas infrastructure in other provinces of China is not yet complete, the  
384 proportion of natural gas would increase significantly in the long run. Unfortunately, there are  
385 currently no results on natural gas leakage rates in other provinces, hindering us from considering  
386 the variations in the natural gas leakage rate between Beijing and other provinces or cities, but we  
387 believe that the calculated natural gas leakage rate can serve as a conservative estimate of China's  
388 natural gas leakage rate in the future.

389

### 390 **3.5 Policy implications**

391 Our observations revealed a strong correlation between methane emissions and natural gas  
392 consumption in terms of both their daily variations and spatial distributions. Generally, the  
393 pressure in natural gas pipelines does not vary with changes in consumption, which suggests that  
394 the amount of natural gas leakage from pipelines remains constant throughout the day. Therefore,



395 our observation results indicated that there was an aging phenomenon in natural gas pipelines in  
396 Beijing. Therefore, it is necessary to implement renovation work for old gas pipelines. In contrast,  
397 the terminal consumption process may drive natural gas leaks in Beijing. Liu et al<sup>41</sup> established a  
398 bottom-up emission inventory and reported that the terminal use process in Beijing accounts for  
399 80% of the total methane emissions in the entire natural gas supply chain. Therefore, the Chinese  
400 government may need to expand the detection of pipeline leaks to the entire natural gas industry  
401 chain.

402 Notably, existing grid-based inventory products also exhibit significant uncertainty in terms  
403 of methane sources. The extracted inventory originates from the Emissions Database for Global  
404 Atmospheric Research (EDGAR) (<https://edgar.jrc.ec.europa.eu/EDGARv8.0>). Although the mean  
405 methane flux ( $126.34 \text{ nmol}\cdot\text{m}^{-2}\cdot\text{s}^{-1}$ ) within the source area is close to our results, the terminal use  
406 process accounts for only approximately 13% of the annual methane emissions, suggesting that  
407 many potential urban methane sources could have been missed, which should be considered in  
408 inventory refinement in the future.

409 In addition, minimizing the methane leakage rate could ensure the early realization of carbon  
410 neutrality in China. Although methane emission control has been included in the agenda for the  
411 first time in the Methane Emission Control Action Plan promulgated in 2023, which clearly  
412 highlights the need to promote the application of leak detection and repair technology and to  
413 enhance the comprehensive recovery and utilization of methane, methane leakage standards have  
414 not been updated. Previous methane leakage standards focused only on controlling the amount of  
415 methane leakage from a safe perspective, thereby ignoring the climate effects of natural gas  
416 leakage. China must urgently develop a strict and detailed set of natural gas leakage standards.

#### 417 **SUPPORTING INFORMATION**

418 Details about the Beijing Meteorological Tower, eddy observation system and navigation  
419 observation station, daily summer variation in CO<sub>2</sub> flux from 2009 to 2017, total consumption,  
420 electricity inflow and the proportion of natural gas in total energy consumption from 2013-2022,  
421 spatial distribution of CO<sub>2</sub> and CH<sub>4</sub> fluxes with wind speed and direction, grid distribution of  
422 natural gas consumption in Beijing, calculation methods of the flux source area and natural gas  
423 leakage rate, uncertainty analysis of flux calculation, estimation of non-natural gas sources

424





425

426 **AUTHOR INFORMATION**

427 **Corresponding Author**

428 **Guiqian Tang** - Key Laboratory of Atmospheric Environment and Extreme Meteorology, Institute  
429 of Atmospheric Physics, Chinese Academy of Sciences, Beijing, 100029, China

430 **Tao Song** - Key Laboratory of Atmospheric Environment and Extreme Meteorology, Institute of  
431 Atmospheric Physics, Chinese Academy of Sciences, Beijing, 100029, China

432 **Authors**

433 **Haoyuan Chen** - Key Laboratory of Atmospheric Environment and Extreme Meteorology,  
434 Institute of Atmospheric Physics, Chinese Academy of Sciences, Beijing, 100029, China

435 **Xiaodong Chen** - Beijing Aozuo Ecological Instrument Co., Ltd., Beijing 100080, China

436 **Yinghong Wang** - Key Laboratory of Atmospheric Environment and Extreme Meteorology,  
437 Institute of Atmospheric Physics, Chinese Academy of Sciences, Beijing, 100029, China

438 **Mengtian Cheng** - Key Laboratory of Atmospheric Environment and Extreme Meteorology,  
439 Institute of Atmospheric Physics, Chinese Academy of Sciences, Beijing, 100029, China

440 **Kai Wang** - Key Laboratory of Atmospheric Environment and Extreme Meteorology, Institute of  
441 Atmospheric Physics, Chinese Academy of Sciences, Beijing, 100029, China

442 **Fuxin Liu** - Anhui University of Science and Technology, Anhui 232001, China

443 **Baoxian Liu** - Beijing Key Laboratory of Airborne Particulate Matter Monitoring Technology,  
444 Beijing Municipal Environmental Monitoring Center, Beijing, 100048, China

445 **Yuesi Wang** - Key Laboratory of Atmospheric Environment and Extreme Meteorology, Institute  
446 of Atmospheric Physics, Chinese Academy of Sciences, Beijing, 100029, China,

447 **ACKNOWLEDGMENTS**

448 This work was supported by the National Key R&D Program of China (2023YFC3706103), the  
449 Strategic Priority Research Program of the Chinese Academy of Sciences (XDB0760200), the  
450 Beijing Municipal Natural Science Foundation (No. 8222075), the Youth Cross Team Scientific  
451 Research Project of the Chinese Academy of Sciences (No. JCTD-2021-10) and the S&T Program  
452 of Hebei (22373903D).

453 **DATA AVAILABILITY**

454 All the data generated or analyzed in this study are included in the published article and are



455 available from the authors upon reasonable request.

#### 456 **AUTHOR STATEMENT**

457 Haoyuan Chen: Formal analysis, methodology, data curation, visualization, and writing—original  
458 draft; Tao Song: methodology and review; Yinghong Wang: methodology and review; Mengtian  
459 Cheng: review; Kai Wang: data curation and review; Fuxin Liu: review; Xiaodong Chen: data  
460 curation and review; Baoxian Liu: data curation and review; Guiqian Tang: supervision, project  
461 administration, funding acquisition, writing—review and editing, and conceptualization; Yuesi  
462 Wang: data curation and review.

463

#### 464 **COMPETING INTERESTS**

465 The authors declare that they have no competing interests.

#### 466 **REFERENCES**

- 467 (1) Environmental Protection Agency. Understanding global warming potentials.  
468 <https://www.epa.gov/ghgemissions/understandingglobal-warming-potentials>.(accessed Oct  
469 22, 2024).
- 470 (2) Kemfert, C.; Präger, F.; Braunger, I.; Hoffart, F. M.; Brauers, H. The expansion of natural gas  
471 infrastructure puts energy transitions at risk. *Nat. Energy*. **2022**, *7*, 582–587 DOI:  
472 s41560-022-01060-3.
- 473 (3) Sargent, M. R.; Floerchinger, C.; McKain, K.; Budney, J.; Gottlieb, E. W.; Hutyra, L. R.;  
474 Wofsy, S. C. Majority of US urban natural gas emissions unaccounted for in inventories.  
475 *Proc. Natl. Acad. Sci.* **2021**, *118* (44), e2105804118 DOI: 10.1073/pnas.2105804118.
- 476 (4) Wunch, D.; Toon, G. C.; Hedelius, J. K.; Vizenor, N.; Roehl, C. M.; Saad, K. M.; Wennberg,  
477 P. O. Quantifying the loss of processed natural gas within California's South Coast Air Basin  
478 using long-term measurements of ethane and methane. *Atmos. Chem. Phys.* **2016**, *16* (22),  
479 14091–14105 DOI: 10.5194/acp-16-14091-2016.
- 480 (5) Frankenberg, C.; Thorpe, A. K.; Thompson, D. R.; Hulley, G.; Kort, E. A.; Vance, N.; Green,  
481 R. O. Airborne methane remote measurements reveal heavy-tail flux distribution in Four  
482 Corners region. *Proc. Natl. Acad. Sci.* **2016**, *113* (35), 9734-9739 DOI:  
483 10.1073/pnas.1605617113.



- 484 (6) Duren, R. M.; Thorpe, A. K.; Foster, K. T.; Rafiq, T.; Hopkins, F. M.; Yadav, V.; Miller, C. E.  
485 California's methane super-emitters. *Nature*. **2019**, *575* (7781), 180-184 DOI:  
486 10.1038/s41586-019-1720-3.
- 487 (7) Sherwin, E. D.; Rutherford, J. S.; Zhang, Z.; Chen, Y.; Wetherley, E. B.; Yakovlev, P. V.;  
488 Brandt, A. R. US oil and gas system emissions from nearly one million aerial site  
489 measurements. *Nature*. **2024**, *627* (8003), 328-334 DOI: 10.1038/s41586-024-07117-5.
- 490 (8) Chen, Z.; Jacob, D. J.; Nesser, H.; Sulprizio, M. P.; Lorente, A.; Varon, D. J.; Yu, X. Methane  
491 emissions from China: a high-resolution inversion of TROPOMI satellite observations.  
492 *Atmos. Chem. Phys.* **2022**, *22* (16), 10809-10826 DOI: 10.5194/acp-22-10809-2022.
- 493 (9) Shen, L.; Jacob, D. J.; Gautam, R.; Omara, M.; Scarpelli, T. R.; Lorente, A.; Lin, J. National  
494 quantifications of methane emissions from fuel exploitation using high resolution inversions  
495 of satellite observations. *Nat Commun.* **2023**, *14* (1), 4948 doi: s41467-023-40671-6.
- 496 (10) Cusworth, D. H.; Jacob, D. J.; Sheng, J. X.; Benmergui, J.; Turner, A. J.; Brandman, J.;  
497 Randles, C. A. (2018). Detecting high-emitting methane sources in oil/gas fields using  
498 satellite observations. *Atmos. Chem. Phys.* **2018**, *18* (23), 16885-16896 DOI:  
499 10.5194/acp-18-16885-2018.
- 500 (11) Barlow, J. F. Progress in observing and modelling the urban boundary layer. *Urban. Clim.*  
501 **2014**, *10*, 216-240 DOI: 10.1016/j.uclim.2014.03.011.
- 502 (12) Undine Z.; Brümmer, C.; Schrader, F.; Ammann, C.; Ibrom, A.; Flechard, C. R.  
503 Surface-atmosphere exchange of ammonia over peatland using QCL-based eddy-covariance  
504 measurements and inferential modeling. *Atmos. Chem. Phys.* **2016**, *16* (17), 11283-11299  
505 DOI: 10.5194/acp-16-11283-2016.
- 506 (13) Lee, X. Handbook of micrometeorology: A Guide for surface Flux Measurement and  
507 Analysis. New York, Kluwer Academic Publishers, 2004.
- 508 (14) Vickers, D.; Mahrt, L. Quality control and flux sampling problems for tower and aircraft data.  
509 *J. Atmos. Ocean. Technol.* **1997**, *14* (3), 512-526 DOI:  
510 10.1175/1520-0426(1997)014<0512:QCAFSP>2.0.CO;2.
- 511 (15) Kaimal, J.C.; Finnigan, J.J. Atmospheric boundary layer flows: their structure and  
512 measurement. Oxford University Press, 1994.
- 513 (16) Fan, S. M.; Wofsy, S. C.; Bakwin, P. S.; Jacob, D. J.; Fitzjarrald, D. R. Atmosphere-biosphere



- 514 exchange of CO<sub>2</sub> and O<sub>3</sub> in the central Amazon forest. *J. Atmos. Ocean. Tech.* **1990**, *95*,  
515 16851-16864 DOI: 10.1029/JD095iD10p16851.
- 516 (17) Webb, E.K.; Pearman, G.I.; Leuning, R. Correction of flux measurements for density effects  
517 due to heat and water vapour transfer. *Q. J. Roy. Meteor. Soc.* **1980**, *106* (447), 85-100 DOI:  
518 10.1002/qj.49710644707.
- 519 (18) Moncrieff, J. B.; Malhi, Y.; Leung, R. The promotion of errors in long term measures of land  
520 atmosphere fluxes of carbon and water. *Global. Change. Biol.* **2010**, *2* (3), 231-240 DOI:  
521 10.5194/acp-15-5987-2010.
- 522 (19) Mauder, M.; Foken T. Documentation and Instruction Manual of the Eddy Covariance  
523 Software Package TK2. *Proc. R. Soc. Met.* 2004, *26* (4), 42-46 DOI:10.5281/zenodo.20349.
- 524 (20) Kljun, N.; Calanca, P.; Rotach, M.W.; Schmid, H.P. A Simple Parameterisation for Flux  
525 Footprint Predictions. *Boundary. Layer. Meteorology.* **2004**, *112* (3), 503-523 DOI:  
526 10.1023/B:BOUN.0000030653.71031.96.
- 527 (21) Kaimal, J. C.; Wyngaard, J. C.; Izumi, Y.; Coté, O. R. Spectral characteristics of surface-layer  
528 turbulence. *Q. J. Roy. Meteor. Soc.* **1972**, *98* (417), 563-589 DOI: 10.1002/qj.49709841707.
- 529 (22) Cheng, X. L.; Liu, X. M.; Liu, Y. J.; Hu, F. Characteristics of CO<sub>2</sub> concentration and flux in  
530 the Beijing urban area. *J. Geophys. Res-Atmos.* **2018**, *123* (3), 1785-1801 DOI:  
531 10.1002/2017JD027409.
- 532 (23) Liu, H. Z.; Feng, J. W.; Järvi, L.; Vesala, T. Four-year (2006–2009) eddy covariance  
533 measurements of CO<sub>2</sub> flux over an urban area in Beijing. *Atmos. Chem. Phys.* **2012**, *12* (17),  
534 7881-7892 DOI: 10.5194/acp-12-7881-2012.
- 535 (24) Liu, Z.; Liu, Z.; Song, T.; Gao, W.; Wang, Y. Long-term variation in CO<sub>2</sub> emissions with  
536 implications for the interannual trend in PM<sub>2.5</sub> over the last decade in Beijing, China.  
537 *Environ. Pollut.* **2020**, *266* (3), 115014. DOI: 10.1016/j.envpol.2020.115014.
- 538 (25) Donato, A.; Conte, M.; Grasso, F.M.; Contini, D. Seasonal and diurnal behaviour of size  
539 segregated particles fluxes in a suburban area. *Atmos. Environ.* **2019**, *219*, 117052 DOI:  
540 10.1016/j.atmosenv.2019.117052.
- 541 (26) Gioli, B.; Toscano, P.; Lugato, E.; Matese, A.; Miglietta, F.; Zaldei, A.; Vaccari, F. P. Methane  
542 and carbon dioxide fluxes and source partitioning in urban areas: The case study of Florence,  
543 Italy. *Environ. Pollut.* **2012**, *164*, 125-131. DOI: 10.1016/J.ENVPOL.2012.01.019.



- 544 (27) Helfter, C.; Tremper, A. H.; Halios, C. H.; Kotthaus, S.; Grimmond, C. S. B. Spatial and  
545 temporal variability of urban fluxes of methane, carbon monoxide and carbon dioxide above  
546 London, UK. *Atmos. Chem. Phys.* **2016**, *16* (16), 10543-10557 DOI:  
547 10.5194/acp-16-10543-2016.
- 548 (28) Pawlak, W.; Fortuniak, K. Eddy covariance measurements of the net turbulent methane flux  
549 in the citycentre – results of 2-year campaign in Łódź, poland. *Atmos. Chem. Phys.* **2016**, *16*  
550 (13), 8281-8294 DOI: /10.5194/acp-16-8281-2016.
- 551 (29) Wang, P.; Zhou, W.; Zhong, X.; Wu, S.; Niu, Z.; Cheng, P.; Hou, Y. Stable carbon isotopic  
552 characteristics of fossil fuels in China. *Sci. Total. Environ.* **2022**, *805*, 150240 DOI:  
553 10.1016/j.scitotenv.2021.150240.
- 554 (30) Wang, P.; Zhou, W.; Xiong, X.; Wu, S.; Niu, Z.; Yu, Y. Source attribution of atmospheric  
555 CO<sub>2</sub> using <sup>14</sup>C and <sup>13</sup>C as tracers in two Chinese megacities during winter. *J. Geophys.*  
556 *Res-Atmos.* **2022**, *127*, e2022JD036504 DOI: 10.1029/2022JD036504.
- 557 (31) Pu, W.; Sheng, J.; Tian, P. On load mobile mapping of spatial variables and source  
558 contributions of ammonia in Beijing, China. *Sci. Total. Env.* **2023**, *864*, 160869 DOI:  
559 10.1016/j.scitotenv.2022.160869.
- 560 (32) Sun, Deng, Wu, Han, Yao. Atmospheric Monitoring of Methane in Beijing Using a Mobile  
561 Observatory. *Atmos.* **2019**, *10* (9), 554 DOI: 10.3390/atmos10090554.
- 562 (33) Lamb, B. K.; Mernanus, J. B.; Shorter, J. H.; Kolb, C. E.; Mosher, B.; Harriss, R. C.  
563 Development of atmospheric tracer methods to measure methane emissions from natural gas  
564 facilities and urban areas. *Environ. Sci. Technol.* **1995**, *29* (6), 1468-1479 DOI:  
565 10.1021/es00006a007.
- 566 (34) Hurry, J.; Risk, D.; Lavoie, M.; Brooks, B. G.; Phillips, C. L.; Göckede, M. Atmospheric  
567 monitoring and detection of fugitive emissions for enhanced oil recovery. *Int. J. Greenh. Gas.*  
568 *Con.* **2016**, *45*, 1-8. DOI: 10.1016/j.ijggc.2015.11.031.
- 569 (35) Cusworth, D. H.; Duren, R. M.; Alana K.; AyasseRalph J. H.; AubreyRobert O.;  
570 GreenMichael L.; EastwoodJohn W.; ChapmanAndrew K.; ThorpeJoseph H. P.;  
571 AsnerMackenzie L.; SmithEben T. J. Quantifying methane emissions from United States  
572 landfills. *Science.* **2024**, *383* (6690), 1499-1504 DOI: 10.1126/science.adi7735.
- 573 (36) Weller, Z.D.; Roscioli, J.R.; Daube, W.C.; Lamb, B.K.; Ferrara, T.W.; Brewer, P.E.



- 574 Vehicle-Based Methane Surveys for Finding Natural Gas Leaks and Estimating Their Size:  
575 Validation and Uncertainty. *Environ Sci Technol.* **2018**, *52* (20), 11922-11930 DOI:  
576 10.1021/acs.est.8b03135.
- 577 (37) Weller, Z. D.; Yang, D. K.; Fischer, J. C. An open source algorithm to detect natural gas leaks  
578 from mobile methane survey data. *PLoS ONE* **2019**, *14* (2), e0212287 DOI:  
579 10.1371/journal.pone.0212287.
- 580 (38) Ars, S.; Vogel, F.; Arrowsmith, C.; Heerah, S.; Wunch, D. Investigation of the Spatial  
581 Distribution of Methane Sources in the Greater Toronto Area Using Mobile Gas Monitoring  
582 Systems. *Environ Sci Technol.* **2020**, *54* (24). DOI: 10.1021/acs.est.0c05386.
- 583 (39) Wang, Y.; Guo, C. H.; Chen, X. J.; Jia, L. Q.; Guo, X. N.; Chen, R. S.; Wang, H. D. Global  
584 climate governance strategies and prospects for China's carbon neutrality path. Forecasting  
585 And Prospects Research Report, 2021.  
586 <https://ceep.bit.edu.cn/docs/2021-01/d714a0f1049d4ed79c881150abfbdc83.pdf>.
- 587 (40) Economics and Development Research Institute. Sinopec, World and China Energy Outlook  
588 2060, 2021.
- 589 (41) Liu, S.; Liu, K.; Wang, K.; Chen, X.; Wu, K. Fossil-fuel and food systems equally dominate  
590 anthropogenic methane emissions in China. *Environ. Sci. Technol.* **2023**, *57* (6), 2495-2505  
591 DOI: 10.1021/acs.est.2c07933.  
592